Electron scattering from optically pumped lithium atoms

V. Karaganov,* Igor Bray, and P. J. O. Teubner
Department of Physics, Electronic Structure of Materials Centre, The Flinders University of South Australia, G.P.O. Box 2100, Adelaide 5001, Australia

(Received 21 October 1997; revised manuscript received 13 August 1998)

A series of superelastic scattering experiments is described in which electrons are scattered from lithium atoms optically pumped to the $2P$ excited state. The incident electron energies were 5.2, 12.2, and 20 eV and superelastically scattered electrons with energies of 7, 14, and 21.8 eV were detected over the angular range from 0° to 140°. Both differential cross sections and the orientation and alignment parameters were deduced from the same measurements. A complete set of the four spin-averaged parameters, which fully characterize the electron impact excitation of the $2S$-$2P$ transition in lithium, is presented. The experimental results are compared with those predicted from convergent-close-coupling (CCC) calculations and two distorted-wave calculations. Excellent agreement is found with the CCC calculations. [S1050-2947(99)06406-9]

PACS number(s): 34.80.Dp, 34.80.Pa, 34.80.Qb

I. INTRODUCTION

The primary motivation for turning our attention to electron-lithium scattering has been the long-standing discrepancy between theory and experiment for the e-H scattering system. Unlike atomic hydrogen, lithium may readily be optically pumped to the excited $2P$ level, thereby allowing the superelastic scattering technique to be used. This technique provides extremely accurate data with which the theory can be compared. It is particularly pleasing to see that the excellent agreement between theory and experiment in the case of lithium [1] was sufficient motivation for new e-H experiments to be performed [2,3]. The new measurements, particularly those of Yalim *et al.* [2], were found to be in agreement with recent most sophisticated theories and not the old measurements.

The measurement of the superelastically scattered signal as a function of the polarization of the laser beam that excites the atom enables both the differential cross sections and the orientation and alignment parameters to be deduced at a particular scattering angle [4]. The orientation and alignment parameters essentially describe the magnitude and phase of the scattering amplitudes and therefore provide an extremely sensitive test of the scattering theory.

The very limited set of experiments that have been reported on electron scattering from lithium reflects the significant technical problems that are encountered in producing beams of lithium atoms. Integral cross sections for the excitation of the $2\,^2P$ state of lithium have been presented by Zapesochnyi *et al.* [5], Leep and Gallagher [6], and Jaduszliwer *et al.* [7]. Differential cross sections have been reported by Williams *et al.* [8] and Vušković *et al.* [9]. The measurements of Vušković *et al.* [9] cover the energy range from 5.4 eV to 200 eV and these results were made absolute by normalization of the angular distributions using a generalized oscillator strength formalism. Shuttleworth *et al.* [10] have measured zero-angle energy-loss spectra for electron scattering from lithium at incident energies from 15 eV to 190 eV. These results have been analyzed to give generalized oscillator strengths and zero-angle differential cross sections for several transitions from the ground state including the $2\,^2P$ transition.

Baum *et al.* [11,12] reported a series of experiments involving polarized electrons and polarized lithium atoms. The spin asymmetry parameter A was measured at several scattering angles for elastic scattering [11] and for the excitation of the $2\,^2P$ state [12] for incident electron energies from 1 eV to 30 eV. Good agreement was found when the measured values of A were compared to those predicted by a 13-state coupled-channel optical calculation of Bray *et al.* [13].

Our initial measurements of the orientation and alignment parameters were reported by Karaganov *et al.* [1,14]. Here we present a complete set of the four spin-averaged parameters, which fully characterize the electron-impact excitation of the $2S$-$2P$ transition in lithium. These parameters include differential cross sections σ, the orientation parameter $L_\perp$, and alignment parameters $\gamma, \overline{P}_{/}$. The present paper also addresses various experimental aspects of the superelastic scattering experiments from lithium in full detail.

Although the apparatus described in this paper was designed to study collisionally induced alignment and orientation phenomena, the differential cross sections for the $2S$-$2P$ transition can also be accurately determined during the same experiment. There are two distinctive techniques by which differential cross sections can be measured using superelastic scattering from optically excited atoms. The method used in the present experiments has been reported previously for small-angle scattering from barium [15–17]. A very different recoil-atom scattering technique has been used by the group at New York University [18] to deduce absolute superelastic differential cross sections for the $3P$-$3S$ transition in sodium.

One the other hand, the measurements of inelastic differential cross sections on alkali-metal and alkali-earth atoms using conventional methods have a long history. Nevertheless, in spite of a large number of measurements reported, there are still substantial discrepancies not only between

*Present address: Jet Propulsion Laboratory, California Institute of Technology, M.S. 183-601, Pasadena, CA 91109.

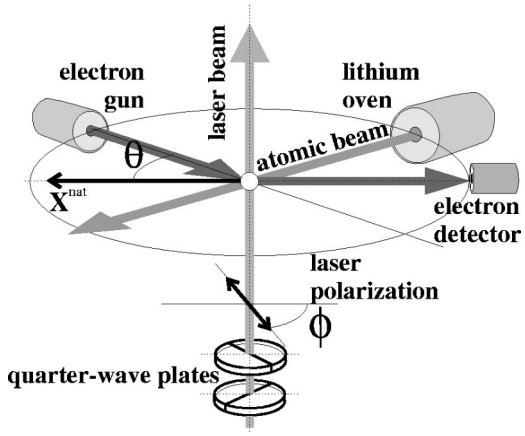

FIG. 1. Schematic diagram showing the experimental geometry and the essential details of the superelastic electron-atom-scattering apparatus.

theories and experiments but also between different sets of experimental data [4,19]. One of the motivations of the present work was to explore the advantages of the superelastic-scattering technique for measurements of differential cross sections for the $2S$-$2P$ transition in lithium.

II. EXPERIMENTAL TECHNIQUES

A. Apparatus

Figure 1 is a schematic diagram of the apparatus. The scattering plane was defined by the directions of the momenta of the incident electrons and the scattered electrons. The electron gun and electron detector could be rotated independently in the scattering plane about the common axis coinciding with the vertically directed laser beam. The range of scattering angles at which measurements could be made was constrained by the physical size of the equipment. Using configurations with different positions of the electron gun and detector, it was possible not only to cover a wide range of scattering angles (up to 140°), but also to check the experimental results for consistency. This was usually achieved by comparison of the data taken for negative and positive scattering angles and/or for different positions of the electron detector.

The size and shape of the scattering volume was defined by the overlap of the laser beam and the atomic beam and could be considered as a cylinder 3 mm in diameter and 3 mm long. This was considerably less than the field of view of the electron detector. It should be noted, however, that this scattering volume could not be treated as infinitely small. The treatment of the systematic errors due to finite angular resolution and volumetric effects are discussed in Sec. II B 4.

The lithium beam was produced in a resistively heated oven. In general, the theory and principles of the design of effusive atomic beam sources are well established [20]. However, specific problems arise in the case of lithium because the solubility and reactivity of molten lithium and lithium vapor become extreme at high temperatures. In such circumstances the performance and reliability of each component of the lithium beam source becomes crucial to the success of the experiments. The typical operating temperature of the oven was 650 °C. Based on the data in Nesmeyanov [21], this resulted in a partial pressure of 0.15 Torr in the oven, which we estimated produced an atomic density of about 5×10^{10} cm^{-3} at the interaction region.

An electron gun with a barium oxide cathode provided the electron beam currents between 0.2 μA and 1 μA. A retarding field electron spectrometer [22] was used to separate the elastically and superelastically scattered electrons. It was found that the overall energy resolution of the system was largely determined by the thermal spread in the incident electron energy. Normally the energy resolution did not exceed 0.3 eV.

A commercial ring dye laser (Spectra-Physics, Model 380D) was used as a source of single-frequency radiation. The laser was tuned to 670.977 nm to optically pump the $2\,^2S_{1/2}$–$2\,^2P_{3/2}$ transition in ^{6}Li. This wavelength was obtained by using DCM laser dye. The dye laser was pumped with a multiline argon ion laser (Coherent, Innova 310). The typical laser power used in the experiments was 300–400 mW. Long-term frequency drifts in the laser were eliminated by locking the laser frequency to the lithium transition [23].

A large fraction of the lithium atoms can become trapped in the ground state during the pumping process. This phenomenon is known as hyperfine-structure trapping. This undesirable effect can be avoided by the simultaneous pumping of both hyperfine ground-state levels. An electro-optic phase modulator was used to generate a number of frequency-shifted sidebands [24]. In the present series of experiments the central frequency and one of the first-order sidebands, separated by 228 MHz, were used to pump the ground-state levels $2\,^2S_{1/2}$, $F=1/2$ and $2\,^2S_{1/2}$, $F=3/2$ simultaneously. The modulation signal was applied as a voltage across electrodes on the top and bottom of an electro-optic $LiTaO_3$ crystal with dimensions of $3\times4\times25$ mm^3 and Z-X-Y orientation. A resonant inductor-capacitor circuit was used to reduce the power of the rf signal required to operate the device. The resonant frequency of the modulators was tuned by changing the physical dimensions of the inductors or capacitors. It was found that optimum pumping conditions were achieved when the oscillator was driven with a rf power of 1 W.

A polarization rotator, consisting of two rotatable quarter-wave plates, was employed in this project in order to obtain either circular polarization or any orientation of linear polarization of the laser radiation required for superelastic experiments. The major advantage of the present scheme over that which had been used before in our laboratory [25] was that it enabled all three components of the Stokes vector to be taken during the same run without changing optical components. This not only significantly reduced the time spent collecting the data, but also completely solved the problem of combining separate measurements when the total polarization P^+, defined in Eq (2.6), was evaluated (Sec. II B 4).

B. Superelastic electron-scattering experiment: Experimental procedure

1. Alignment and orientation parameters

For the experimental geometry shown in Fig. 1, where the laser propagates perpendicular to the scattering plane, the reduced Stokes parameters measured in superelastic electron scattering experiments are defined as [26]:

$$\overline{P}_1(\theta)=\frac{1}{K}P_1(\theta),$$

$$\overline{P}_2(\theta)=\frac{1}{K}P_2(\theta), \tag{2.1}$$

$$\overline{P}_3(\theta)=\frac{1}{K'}P_3(\theta),$$

where

$$P_1(\theta)=\frac{I_0(\theta)-I_{90}(\theta)}{I_0(\theta)+I_{90}(\theta)},$$

$$P_2(\theta)=\frac{I_{45}(\theta)-I_{135}(\theta)}{I_{45}(\theta)+I_{135}(\theta)}, \tag{2.2}$$

$$P_3(\theta)=\frac{I_{RHC}(\theta)-I_{LHC}(\theta)}{I_{RHC}(\theta)+I_{LHC}(\theta)}.$$

In Eqs. (2.2), $I_\phi(\theta)$ denotes the count rate of the superelastically scattered electrons when the laser is linearly polarized at the angle of ϕ, with respect to the direction of the scattered electrons, or when the laser is right-left-handed circularly polarized. θ denotes the scattering angle. K and K' are the superelastic depolarization factors associated with linear and circular optical pumping [26]. The reduced Stokes components are related to the alignment, orientation, and coherence parameters as [27]

$$L_\perp=-\overline{P}_3, \tag{2.3}$$

$$\overline{P}_\nearrow=\sqrt{\overline{P}_1^2+\overline{P}_2^2}, \tag{2.4}$$

$$\gamma=\frac{1}{2}\arg(\overline{P}_1+i\overline{P}_2), \tag{2.5}$$

$$P^+=\sqrt{\overline{P}_1^2+\overline{P}_2^2+\overline{P}_3^2}. \tag{2.6}$$

The six different states of polarization of the laser radiation were obtained using the dual wave plate polarization rotator. The laser beam was chopped at 61 Hz with a rotating toothed wheel and the count rates $I_\phi(\theta)$ were determined using gated counters. The typical superelastic signal count rate varied from 10 Hz to 10 kHz and it depended on the incident electron energy, the beam current, and the scattering angle. The background count rate usually did not exceed 1–10 % of the signal.

The Stokes parameters for each scattering angle were measured several times at different positions of the electron detector and electron gun. This procedure minimized the influence of the systematic errors.

The entire experiment was controlled by the computer, though human supervision was required to provide readjustment to the laser frequency in the case of mode hops. The total acquisition time varied from several minutes to several hours at each angle.

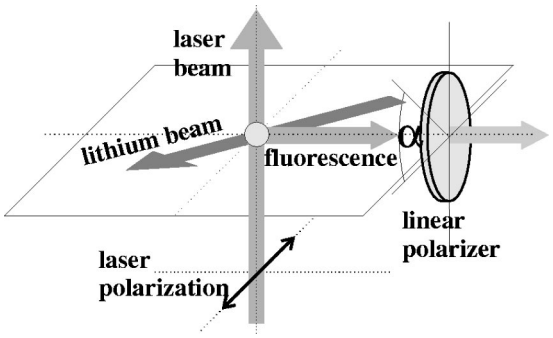

FIG. 2. Schematic diagram of the experimental geometry used in the line polarization measurements during optical pumping with the linearly polarized light.

2. Optical pumping and fluorescence measurement

Determination of the superelastic depolarization factors K and K' was essential for interpretation of the experimental results. As discussed by Farrell *et al.* [26] and Meng *et al.* [28], the factor K was taken to be identical to the line polarization of the resonant fluorescence P_L. For the geometry shown in Fig. 2 the line polarization P_L is defined as

$$P_L=\frac{\mathcal{F}(0°)-\mathcal{F}(90°)}{\mathcal{F}(0°)+\mathcal{F}(90°)}, \tag{2.7}$$

where $\mathcal{F}(\alpha)$ is the intensity of the fluorescence signal that is analyzed by a linear polarizer [28]. This signal was monitored through the vacuum window during the experiment, so it was possible to determine the factor $K=P_L$ for each measurement.

A series of experiments has been conducted previously [29] to study the optical pumping processes in lithium. The measured data were useful in the subsequent superelastic scattering experiments since the pumping conditions could be optimized on the basis of this knowledge. The QED model [26] predicts excited-state densities of about 17% for ^{6}Li and 8% for ^{7}Li at laser intensities of 20 mW/mm^2 [30]. Although it is possible to conduct superelastic-scattering experiments under these conditions, it is preferable to increase the excited-state population using the dual-frequency pump-

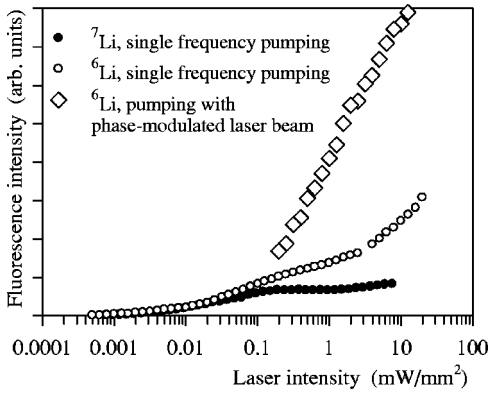

FIG. 3. Comparison of the different ways of optical pumping. ○ and ● represent the fluorescent intensity as a function of laser intensity measured for single-frequency pumping. ◇ represents the fluorescent intensity as a function of laser intensity measured for dual-frequency pumping with a phase-modulated laser beam.

ing technique. The advantage of dual-frequency optical pumping can be clearly seen from the experimental data presented in Fig. 3. The use of the electro-optic modulator allowed a substantial increase in the excited-state population.

The dependence of P_L on various experimental conditions has been investigated [29]. The results of these measurements showed that P_L was essentially constant over a wide range of laser intensities. Specifically it was found that

$$P_L = 0.575 \pm 0.010 \tag{2.8}$$

when the intensity of the pumping radiation in the interaction region changed from 5 $\mathrm{mW/mm^2}$ to 40 $\mathrm{mW/mm^2}$. In contrast, the uncertainty in P_L in the case of ^{7}Li was substantially greater. This remarkable insensitivity of P_L to the experimental conditions was one of the reasons why the ^{6}Li isotope has been chosen for further experiments.

The factor K' characterizes the depolarization in the case of circularly polarized optical pumping and, in principle, plays an equally important role in the determination of $\overline{P}_3$. It is shown in the literature, however, that this parameter is practically independent of the experimental conditions and is very close to unity at any laser intensities except at very low levels [26]. In practice, the measurement of K' requires the determination of the degree of circular polarization of the fluorescence at a very small angle to the laser beam [26]. This measurement is difficult to perform and is usually associated with large errors. Thus, in the present project the theoretically calculated value $K' \approx 1$ was used for the evaluation of the Stokes parameter $\overline{P}_3$. The experimental results for $P_3(\theta)$ (Fig. 5) give an additional confirmation that the assumption $K' \approx 1$ is justified. We can write from general considerations

$$\frac{P_3}{K'} = \overline{P}_3 \leqslant 1, \quad K' \leqslant 1. \tag{2.9}$$

On the other hand, the maximum measured value of P_3,

$$P_3 = 0.986 \pm 0.033, \tag{2.10}$$

was observed experimentally at 20 eV at the scattering angle of 80°. Thus the meaningful range for K' can be determined from Eqs. (2.9) and (2.10) as

$$1 \geqslant K' \geqslant 0.986 \pm 0.033. \tag{2.11}$$

3. Differential cross sections

The theoretical analysis of the electron scattering from the laser excited atomic target is given in [4,31]. It has been shown that for the experimental geometry where the laser beam is perpendicular to the scattering plane (Fig. 1) the angular distribution of the total scattering intensities $I_{lin}(\theta)$ and $I_{circ}(\theta)$ is dependent only on the differential cross section $\sigma(\theta)$:

$$I_{lin}(\theta) = I_0(\theta) + I_{90}(\theta) = I_{45}(\theta) + I_{135}(\theta) \propto \sigma(\theta), \tag{2.12}$$

$$I_{circ}(\theta) = I_{RHC}(\theta) + I_{LHC}(\theta) \propto \sigma(\theta). \tag{2.13}$$

The above analysis assumes a positive reflection symmetry in the excited P state. This implies that $\rho_{00}^{nat} \equiv 0$, where ρ_{00}^{nat} is a density matrix element in the natural frame [4,31]. It is also assumed that the optical pumping conditions are constant during a measurement.

This allows the relative differential cross section (DCS) to be determined from the measured superelastic-scattering count rates at different polarizations of the laser radiation. It is clear that in our case the differential cross sections can be determined simultaneously with the Stokes parameters (Sec. II B).

Considering the problem of DCS measurement, we note that the superelastic technique, when applicable, provides several clear advantages when compared to the conventional technique. In superelastic experiments an interaction volume is defined by an intersection of the laser beam and the atomic beam (Fig. 1); this is much better than in inelastic experiments where poorly collimated electron and atomic beams determine the collision region. The density of excited atoms in the interaction region can be monitored by observing a spontaneous fluorescence signal, which is technically easier than measuring a density of neutral atoms. The background can be readily determined and subtracted from the signal simply by chopping the laser beam.

When the conventional technique is used, it is often difficult to discriminate inelastic peaks in an energy-loss spectrum because the energy separations between the P, D, and F states can be comparable to or smaller than the resolution of the measuring system. Unlike the inelastic peaks, the superelastic peak is well separated from both the elastic and inelastic features. In addition, the superelastic electrons have a higher energy and can be detected with an efficient retarding field analyzer.

4. Experimental uncertainties

An extensive study has been undertaken in order to identify, qualitatively estimate, and possibly remove various systematic errors including those due to finite angular resolution, imperfect laser polarization, scattering angle determination, radiation trapping, and electron energy variation.

The scattering angle was the independent variable in this project. Consequently, it was important that the electron-scattering angle was accurately determined. The residual magnetic field in the interaction region was less than 3 mG, so its influence could be neglected. However, static electric fields created by oil deposits from the diffusion pump could cause problems at low incident electron energies. Thus alignment of the electron gun and detector using conventional mechanical means was often not sufficient to ensure correct determination of the true zero-scattering angle. It was therefore necessary to check the preliminary mechanical alignment by measuring the position of the extremum on the $\overline{P}_1(\theta)$ curve exactly corresponding to $\theta = 0°$.

Two further tests were also important. First, the symmetry of the results for negative and positive scattering angles was checked at large angles. Second, the experimental data taken for the same scattering angle but for different positions of the gun and electron detector with respect to the central vertical axis were checked for consistency. The X^{nat} axis for superelastic-scattering experiment is parallel to the direction

of the scattered electron [4]. Thus good practice dictates that the scattered electron detector remains fixed and the scattering angle is changed by rotating the electron gun. A complete set of data was taken for the appropriate scattering angles with the detector fixed in one position. The detector was then rotated by 45° and the experiments repeated. It was observed that these results were consistent with the first set of data. Similar results were obtained when the detector was rotated by 90° from the original position. Such consistency checks were performed regularly during the course of the experiments and they indicated that the confidence in the scattering angle was better than $\pm 1.5°$ over the whole range of angles.

When $\overline{P}_1$, $\overline{P}_2$, and $\overline{P}_3$ are measured in two separate experiments an additional systematic error in P^+ can arise from possible uncertainties in the determination of the true scattering angle in each case [29]. Even a small angular offset may result in large changes of P^+ due to rapid variations in the Stokes parameters at certain angles. Model calculations have been carried out in order to simulate this effect. The result of such modeling demonstrates that combining the measurements for $\overline{P}_1(\theta)$, $\overline{P}_2(\theta)$, and shifted $\overline{P}_3(\theta-1.5°)$ gives a discrepancy of up to 16% in the total polarization P^+ and may result in a strongly pronounced artificial structure. The type of polarization rotator used in the present experiments allowed all three Stokes components to be determined simultaneously. This removed any potential angular shift between the measurements of $\overline{P}_1$, $\overline{P}_2$, and $\overline{P}_3$ and thus completely eliminated the problem.

The finite angular resolution and finite interaction volume are factors that must be taken into account when comparing the experimental results with the theoretical calculations. Discussions addressing these problems and several examples of their solution can be found in the literature [32–35]. In our case these effects were simulated by performing the convolution transform with appropriate normalization [32]

$$\langle P_i(\theta)\rangle = \frac{(P_i\sigma)*H}{\sigma*H} = \frac{\int_{-\infty}^{+\infty} P_i(\theta')\sigma(\theta')H(\theta-\theta')d\theta'}{\int_{-\infty}^{+\infty} \sigma(\theta')H(\theta-\theta')d\theta'}, \quad (2.14)$$

Here P_i and σ represent the corresponding theoretical data for the Stokes parameters and differential cross section. The function $H(\theta)$ characterizes the overall angular resolution of the measuring system and, in our case, is taken to be Gaussian with an angular width of 3° full width at half maximum.

Equation (2.14) is applicable for modeling the influence of the finite angular resolution and the volumetric effects when only collision events within the scattering plane are considered. Extension of the finite interaction volume out of the scattering plane leads to an effective rotation of the scattering plane about the X^{nat} axis and therefore to a different geometry of the measurements. This situation was discussed by Zetner *et al.* [34] and more recently by Sang *et al.* [36,37]. Modeling calculations based on the formalism given in [36,37] demonstrates that the ''out-of-plane'' effects are pronounced only at small angles and in our case their influence is less significant than the influence of the ''in-plane'' effects.

An accurate knowledge of the electron energy is required to minimize possible systematic errors due to instabilities of the electron gun characteristics. An electron energy calibration facility was established in the scattering chamber to enable the electron beam energy to be measured and corrected (if necessary) any time during the experiment without opening the chamber and changing the experimental arrangement. The beam energy was calibrated against the *b* feature in the metastable excitation function of neon, which is at 16.906 eV [38].

Experimentally measured values of the Stokes parameters and the line polarization can be underestimated when the density of atoms in the interaction region is too high. This problem arises from radiation trapping where the absorption and reemission of photons in the interaction region results in substantial depolarization of the target at large atomic beam densities. Kadota *et al.* [39] checked the influence of radiation trapping in their experiments with optically excited lithium atoms and found it to be still negligibly small up to a density of 1.5×10^{12} cm^{-3}. It was estimated that in our case the lithium beam density did not exceed 8×10^{10} cm^{-3}. Therefore, it is expected that depolarization due to radiation trapping will be small under the conditions of the experiment. The oven used in the present experiments could not be heated above 700 °C. Consequently, we were unable to demonstrate the onset of radiation trapping. Nevertheless, we were able to show that both the Stokes parameters and the line polarization were independent of the atomic beam density when the fluorescence signal and hence the atomic density changed by a factor of about 50. The variation in atomic beam density was monitored by the fluorescence signal. No variation of the measured Stokes parameters or variation of the line polarization P_L beyond the typical statistical uncertainties was detected, so we conclude that our results are free from radiation trapping effects.

The experiments were carried out with the assumption that the excited states of lithium atoms were prepared by the laser radiation in ''pure'' polarization states. If this was not the case, the presence of a residual elliptical polarization of the pumping laser beam could cause serious systematic errors in measurements of the Stokes parameters. In a practical experiment such small elliptical components in the laser radiation could appear because of the imperfections or misalignment of the quarter-wave plates or the birefringence of the vacuum window.

Detailed theoretical and experimental studies of the polarization-related problems in superelastic experiments will be reported elsewhere [40]. It can be shown that given the error in the laser polarization state, the uncertainty ΔP_i in the Stokes parameters can be qualitatively estimated. In particular, it was found that when measuring electron scattering for linearly polarized light (P_1,P_2), the errors are proportional to the admixture of undesirable circular polarization and to P_3.

For the present series of experiments the degree of polarization of the incident laser beam was measured and found to

TABLE I. Differential cross sections σ and reduced Stokes parameters $\overline{P}_1, \overline{P}_2, \overline{P}_3$ measured for an electron energy of 7 eV referred to the ground state.

θ (deg)	σ ($cm^2\ sr^{-1}$)	$\overline{P}_1$	$\overline{P}_2$	$\overline{P}_3$
0	2.91×10^{-14}	0.863 ± 0.040	-0.185 ± 0.127	-0.019 ± 0.005
2	2.60×10^{-14}	0.751 ± 0.038	-0.290 ± 0.091	-0.048 ± 0.022
4	2.05×10^{-14}	0.646 ± 0.104	-0.539 ± 0.049	-0.091 ± 0.026
6	1.83×10^{-14}	0.344 ± 0.066	-0.837 ± 0.080	-0.153 ± 0.018
8	1.36×10^{-14}	-0.017 ± 0.115	-0.950 ± 0.046	-0.251 ± 0.008
10	1.17×10^{-14}	-0.230 ± 0.071	-0.875 ± 0.031	-0.258 ± 0.036
12	8.33×10^{-15}	-0.395 ± 0.081	-0.813 ± 0.047	-0.367 ± 0.043
14	5.90×10^{-15}	-0.525 ± 0.120	-0.767 ± 0.102	-0.470 ± 0.032
16	3.82×10^{-15}	-0.607 ± 0.184	-0.459 ± 0.075	-0.449 ± 0.090
18	2.72×10^{-15}	-0.734 ± 0.063	-0.499 ± 0.028	-0.500 ± 0.031
20	2.01×10^{-15}	-0.619 ± 0.026	-0.452 ± 0.030	-0.543 ± 0.021
25	9.92×10^{-16}	-0.610 ± 0.022	-0.303 ± 0.028	-0.655 ± 0.012
30	4.83×10^{-16}	-0.427 ± 0.028	-0.180 ± 0.019	-0.819 ± 0.024
35	2.61×10^{-16}	-0.107 ± 0.080	-0.167 ± 0.024	-0.901 ± 0.006
40	1.74×10^{-16}	0.228 ± 0.052	-0.288 ± 0.014	-0.856 ± 0.017
45	1.25×10^{-16}	0.410 ± 0.016	-0.495 ± 0.030	-0.739 ± 0.013
50	1.03×10^{-16}	0.488 ± 0.021	-0.635 ± 0.027	-0.577 ± 0.007
55	9.33×10^{-17}	0.500 ± 0.018	-0.720 ± 0.025	-0.491 ± 0.006
60	8.14×10^{-17}	0.525 ± 0.025	-0.720 ± 0.035	-0.445 ± 0.008
65	7.12×10^{-17}	0.540 ± 0.023	-0.678 ± 0.037	-0.441 ± 0.013
70	5.80×10^{-17}	0.518 ± 0.026	-0.607 ± 0.065	-0.454 ± 0.011
75	4.63×10^{-17}	0.567 ± 0.028	-0.599 ± 0.050	-0.499 ± 0.008
80	3.77×10^{-17}	0.621 ± 0.031	-0.502 ± 0.045	-0.516 ± 0.008
85	2.95×10^{-17}	0.657 ± 0.026	-0.378 ± 0.040	-0.542 ± 0.010
90	2.07×10^{-17}	0.672 ± 0.036	-0.183 ± 0.058	-0.565 ± 0.010
95	1.53×10^{-17}	0.636 ± 0.032	0.002 ± 0.044	-0.568 ± 0.005
100	1.11×10^{-17}	0.508 ± 0.037	0.206 ± 0.028	-0.447 ± 0.020
105	1.01×10^{-17}	0.349 ± 0.121	0.273 ± 0.024	-0.157 ± 0.106
110	8.82×10^{-18}	0.319 ± 0.011	0.258 ± 0.079	0.140 ± 0.064
115	8.65×10^{-18}	0.189 ± 0.024	0.113 ± 0.055	0.474 ± 0.016
120	1.12×10^{-17}	0.263 ± 0.060	-0.196 ± 0.078	0.666 ± 0.029
125	1.51×10^{-17}	0.379 ± 0.068	-0.263 ± 0.044	0.729 ± 0.026
130	1.71×10^{-17}	0.532 ± 0.053	-0.464 ± 0.052	0.670 ± 0.004
135	1.91×10^{-17}	0.602 ± 0.093	-0.441 ± 0.034	0.570 ± 0.025
140	2.47×10^{-17}	0.669 ± 0.018	-0.407 ± 0.009	0.559 ± 0.011

be better than 0.9996 using the Stokes formalism [41] where perfect polarization is identically 1. Nevertheless, it can be shown [40] that this level of uncertainty in the laser beam polarization can give rise to uncertainties in the Stokes parameters defined in Eqs. (2.2) that are estimated to be

$$|\Delta P_{1,2}| \leqslant 0.065, \quad |\Delta P_3| \leqslant 0.007. \tag{2.15}$$

It should be mentioned that these estimates present only the upper limits of the expected uncertainties. However, in some cases they were essentially zero. For example, in the measurement of $\overline{P}_1$ the systematic error due to a small circular component may add for positive electron-scattering angles and subtract for negative angles. This situation arises because $\overline{P}_1$ is symmetric about $\theta = 0°$, whereas $\overline{P}_3$ is antisymmetric. Consequently, when two sets of results are averaged for positive and negative scattering angles the systematic errors from the two effects cancel. Therefore it is difficult to cite a precise value of the systematic errors at each angle and all the errors quoted in Tables I–III and Fig. 5 are statistical and represent plus and minus one standard deviation.

We note that an error analysis [40] confirms the intuitive view that the parameter $\overline{P}_3$ is the least sensitive component of the Stokes vector to the systematic polarization problems. It is also clear from our measurements that $\overline{P}_3$ is virtually unaffected by finite angular resolution effects since there is no sharp structure in this parameter over the whole range of scattering angles.

III. THEORY

The details of the convergent close-coupling (CCC) theory suitable for electron-lithium-scattering calculations

TABLE II. Differential cross sections σ and reduced Stokes parameters $\overline{P}_1, \overline{P}_2, \overline{P}_3$ measured for an electron energy of 14 eV referred to the ground state.

θ (deg)	σ ($cm^2\ sr^{-1}$)	$\overline{P}_1$	$\overline{P}_2$	$\overline{P}_3$
0	6.10×10^{-14}	0.756 ± 0.025	-0.124 ± 0.043	-0.006 ± 0.005
1	5.91×10^{-14}	0.670 ± 0.032	-0.385 ± 0.043	-0.036 ± 0.012
2	5.31×10^{-14}	0.527 ± 0.053	-0.597 ± 0.060	-0.055 ± 0.008
3	4.46×10^{-14}	0.338 ± 0.083	-0.750 ± 0.056	-0.086 ± 0.001
4	3.95×10^{-14}	0.073 ± 0.008	-0.853 ± 0.021	-0.108 ± 0.004
5	2.99×10^{-14}	0.009 ± 0.013	-0.894 ± 0.027	-0.136 ± 0.008
6	2.39×10^{-14}	-0.311 ± 0.012	-0.852 ± 0.022	-0.157 ± 0.004
8	1.46×10^{-14}	-0.557 ± 0.018	-0.723 ± 0.022	-0.206 ± 0.005
10	9.00×10^{-15}	-0.701 ± 0.022	-0.579 ± 0.022	-0.264 ± 0.006
12	5.66×10^{-15}	-0.791 ± 0.026	-0.450 ± 0.023	-0.297 ± 0.008
14	3.68×10^{-15}	-0.833 ± 0.026	-0.380 ± 0.023	-0.340 ± 0.008
16	2.25×10^{-15}	-0.832 ± 0.029	-0.298 ± 0.026	-0.411 ± 0.010
18	1.46×10^{-15}	-0.812 ± 0.033	-0.285 ± 0.031	-0.469 ± 0.012
20	9.79×10^{-16}	-0.768 ± 0.039	-0.250 ± 0.025	-0.524 ± 0.027
25	3.79×10^{-16}	-0.585 ± 0.047	-0.240 ± 0.010	-0.720 ± 0.021
30	1.62×10^{-16}	-0.241 ± 0.023	-0.305 ± 0.020	-0.857 ± 0.006
35	9.15×10^{-17}	0.074 ± 0.018	-0.496 ± 0.027	-0.817 ± 0.010
40	6.33×10^{-17}	0.256 ± 0.018	-0.661 ± 0.045	-0.666 ± 0.017
45	5.14×10^{-17}	0.350 ± 0.032	-0.733 ± 0.042	-0.542 ± 0.008
50	4.05×10^{-17}	0.401 ± 0.022	-0.738 ± 0.032	-0.492 ± 0.005
55	2.89×10^{-17}	0.450 ± 0.020	-0.729 ± 0.030	-0.485 ± 0.007
60	2.02×10^{-17}	0.541 ± 0.022	-0.634 ± 0.022	-0.515 ± 0.004
65	1.39×10^{-17}	0.644 ± 0.027	-0.455 ± 0.030	-0.563 ± 0.004
70	9.28×10^{-18}	0.780 ± 0.036	-0.218 ± 0.036	-0.582 ± 0.007
75	6.11×10^{-18}	0.810 ± 0.032	0.089 ± 0.037	-0.549 ± 0.010
80	4.14×10^{-18}	0.738 ± 0.028	0.523 ± 0.039	-0.307 ± 0.027
85	3.39×10^{-18}	0.412 ± 0.018	0.753 ± 0.040	0.152 ± 0.025
90	3.27×10^{-18}	0.080 ± 0.041	0.542 ± 0.035	0.639 ± 0.023
95	3.98×10^{-18}	-0.079 ± 0.029	0.109 ± 0.031	0.895 ± 0.010
100	5.16×10^{-18}	-0.056 ± 0.032	-0.259 ± 0.031	0.919 ± 0.004
105	6.67×10^{-18}	0.011 ± 0.036	-0.424 ± 0.050	0.858 ± 0.009
110	8.80×10^{-18}	0.185 ± 0.050	-0.596 ± 0.049	0.787 ± 0.021
115	1.07×10^{-17}	0.303 ± 0.042	-0.682 ± 0.038	0.696 ± 0.021
120	1.26×10^{-17}	0.406 ± 0.083	-0.679 ± 0.030	0.608 ± 0.028
125	1.43×10^{-17}	0.481 ± 0.014	-0.692 ± 0.018	0.555 ± 0.022
130	1.62×10^{-17}	0.616 ± 0.047	-0.67 ± 0.032	0.499 ± 0.025
135	1.79×10^{-17}	0.638 ± 0.044	-0.602 ± 0.018	0.439 ± 0.011

have already been given [42]. Briefly, the method is based on the close-coupling formalism involving the solution of coupled Lippmann-Schwinger equations. These are derived by expanding the total wave function using a set of N negative- and positive-energy target states obtained by diagonalizing the target Hamiltonian in an orthogonal Laguerre basis. The use of such a basis ensures that simply with increasing N the expansion yields an increasingly accurate description of the target discrete and continuous spectrum.

The method concentrates on treating the scattering aspect of the calculation, leaving the primary approximation being the treatment of the target structure. Presently, the lithium atom is modeled using the frozen-core Hartree-Fock model. The two core $1s$ electrons are assumed to be inert and are used to define the Hartree-Fock potential governing the motion of the valence electron. Lithium is particularly well suited to such a description. For the heavier alkali metals we find that this model also works very well with the addition of a phenomenological core-polarization potential [42], but we do not require this here.

The total number of expansion states is given by $N=\Sigma_l N_l$, where l ranges up to $l_{\max}$. Thus a test of convergence requires the increase of both $l_{\max}$ and N_l within each l. The size of the calculations typically depends on the relative size of the cross sections being calculated. The $2P$ excitation of lithium is one of the largest lithium cross sections and so the numerical analysis is relatively simple. Convergence with $l_{\max}$ is found at $l_{\max}=3$ and we typically have $N_l=13-l$.

In addition, we performed a standard close-coupling (CC)

TABLE III. Differential cross sections σ and reduced Stokes parameters $\overline{P}_1, \overline{P}_2, \overline{P}_3$ measured for an electron energy of 21.8 eV referred to the ground state.

θ (deg)	σ ($cm^2\ sr^{-1}$)	$\overline{P}_1$	$\overline{P}_2$	$\overline{P}_3$
6		-0.585 ± 0.067	-0.692 ± 0.071	-0.126 ± 0.024
10		-0.878 ± 0.043	-0.419 ± 0.038	-0.207 ± 0.009
12	2.67×10^{-15}	-0.890 ± 0.057	-0.367 ± 0.055	-0.271 ± 0.041
14	2.10×10^{-15}	-0.894 ± 0.021	-0.242 ± 0.010	-0.320 ± 0.003
16	1.19×10^{-15}	-0.877 ± 0.021	-0.210 ± 0.010	-0.393 ± 0.003
18	6.61×10^{-16}	-0.830 ± 0.031	-0.198 ± 0.011	-0.441 ± 0.032
20	3.95×10^{-16}	-0.825 ± 0.031	-0.201 ± 0.011	-0.549 ± 0.017
25	1.10×10^{-16}	-0.491 ± 0.018	-0.237 ± 0.014	-0.781 ± 0.004
30	5.09×10^{-17}	-0.234 ± 0.038	-0.425 ± 0.036	-0.838 ± 0.004
35	3.06×10^{-17}	0.214 ± 0.014	-0.570 ± 0.022	-0.733 ± 0.005
40	1.67×10^{-17}	0.264 ± 0.033	-0.699 ± 0.038	-0.589 ± 0.009
45	1.11×10^{-17}	0.537 ± 0.028	-0.709 ± 0.031	-0.504 ± 0.009
50	8.20×10^{-18}	0.580 ± 0.062	-0.652 ± 0.027	-0.450 ± 0.014
55	5.10×10^{-18}	0.778 ± 0.050	-0.468 ± 0.036	-0.374 ± 0.013
60	3.18×10^{-18}	0.962 ± 0.046	-0.160 ± 0.044	-0.239 ± 0.021
65	2.19×10^{-18}	0.989 ± 0.065	0.141 ± 0.053	0.085 ± 0.036
70	1.79×10^{-18}	0.822 ± 0.052	0.324 ± 0.080	0.480 ± 0.044
75	1.78×10^{-18}	0.475 ± 0.146	0.326 ± 0.050	0.801 ± 0.040
80	1.77×10^{-18}	0.078 ± 0.064	-0.006 ± 0.044	0.986 ± 0.033
85	2.04×10^{-18}	0.056 ± 0.078	-0.217 ± 0.032	0.965 ± 0.013
90	2.25×10^{-18}	-0.038 ± 0.048	-0.425 ± 0.038	0.894 ± 0.015
95	2.57×10^{-18}	0.081 ± 0.045	-0.536 ± 0.036	0.795 ± 0.014
100	2.91×10^{-18}	0.080 ± 0.043	-0.651 ± 0.034	0.733 ± 0.011
105	3.42×10^{-18}	0.188 ± 0.126	-0.815 ± 0.044	0.657 ± 0.028
110	3.81×10^{-18}	0.280 ± 0.049	-0.698 ± 0.070	0.575 ± 0.060
115	3.94×10^{-18}	0.353 ± 0.148	-0.797 ± 0.063	0.527 ± 0.056
120	4.43×10^{-18}	0.459 ± 0.081	-0.764 ± 0.045	0.493 ± 0.033
125	5.22×10^{-18}	0.579 ± 0.056	-0.738 ± 0.054	0.412 ± 0.026
130	5.32×10^{-18}	0.674 ± 0.054	-0.699 ± 0.052	0.382 ± 0.020
135	5.68×10^{-18}	0.697 ± 0.062	-0.651 ± 0.065	0.330 ± 0.021
140	5.95×10^{-18}	0.828 ± 0.046	-0.608 ± 0.067	0.286 ± 0.014

calculation that is convergent in treating of just the discrete target eigenstates. States with $n\leqslant7$ were included.

IV. RESULTS AND DISCUSSION

The reduced spin-averaged Stokes parameters $\overline{P}_1, \overline{P}_2, \overline{P}_3$ are given in Table I–III at the three incident energies 7, 14, and 21.8 eV referred to the ground state. The uncertainties quoted represent one standard deviation. The differential cross sections are also presented in the tables. The data in these tables provide a complete set of the four spin-averaged parameters that fully characterize the electron-impact excitation of the $2P$ transition in lithium from the ground state.

The previously reported experimental data available for comparison are the DCS measured in conventional inelastic-scattering experiments [8,9] for an electron energy of 20 eV. The present relative differential cross sections were extracted from the measurements of the superelastic-scattering intensities as described in Sec. II B 3. The normalization method employed in the present work involved integrating the measured DCS over a range of scattering angles from 0° to 140° with subsequent normalizing to a known value of the integrated cross section for the $2S$-$2P$ transition in lithium. This method was used to normalize the DCS measurements at 7 eV and 14 eV.

The integrated cross sections given by Leep and Gallagher [43] were used in the described normalization procedure. We note that the values reported by Leep and Gallagher [43] have been confirmed by a number of subsequent independent measurements [5,8,9]. The accuracy of the reported integrated cross sections varied from 10% to 35%.

No measurements have been performed in the present project at small scattering angles for 21.8 eV. This region is particularly important for normalization because the differential cross section is strongly peaked for the forward angles. Thus it was not possible to obtain an accurate integral cross section at this energy. In order to compare the relative values of differential cross section, our results for 21.8 eV have been normalized to the value of DCS at the point where the theory is in good agreement with the measurements by Vušković *et al.* [9], which is at a scattering angle of 14°.

The absolute values of differential cross sections mea-

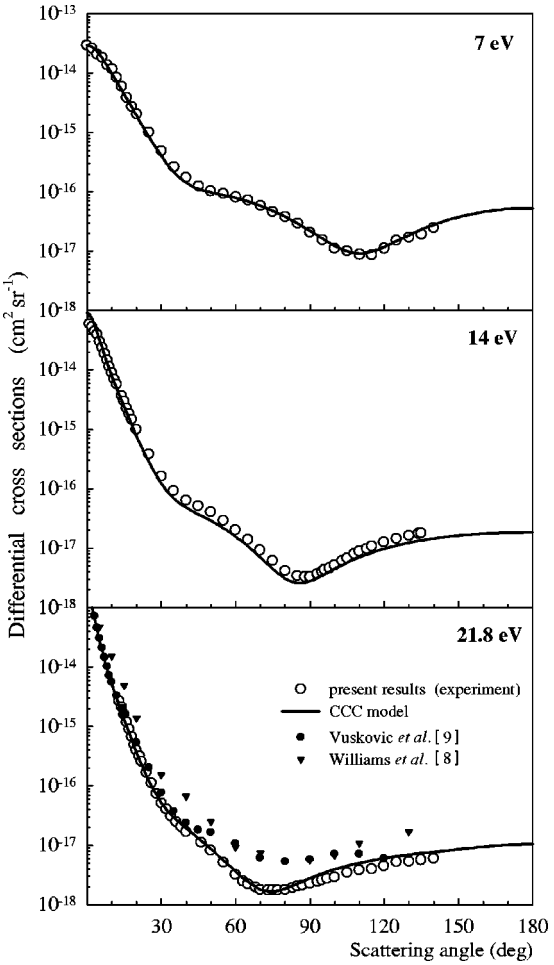

FIG. 4. Differential cross sections for the $2S$-$2P$ transition at electron energies of 7, 14, and 21.8 eV referred to the ground state. The measurements by Williams *et al.* [8] and Vušković *et al.* [9] are given for an electron energy of 20 eV.

sured at 7 eV and 14 eV and relative measurements at 21.8 eV are presented in Fig. 4. Agreement between the present set of experimental data and the CCC calculations is good at all scattering angles and for all energies.

The measurements published by Williams *et al.* [8] and by Vušković *et al.* [9] for 20 eV give larger absolute values of the DCS than those predicted by the theory. However, if one considers only the angular distributions and ignores the problems of normalization, it can be seen that there is reasonable agreement between experiment and theory with respect to shape.

While differential cross sections provide an important test of the theoretical predictions, a more detailed comparison can be drawn using the orientation and alignment parameters. These parameters can be derived from the data in Tables I–III using Eqs. (2.3)–(2.6). The derived parameters $L_\perp$, γ, $\overline{P_\ell}$, and P^+ are shown in Fig. 5.

As was discussed previously in Sec. II B, the finite angular resolution and finite interaction volume are factors that should be taken into account when comparing the present results with the theoretical calculations. These effects were simulated by performing the convolution transform (2.14) of the corresponding CCC data and the Gaussian function that characterizes the instrumental effects. The experimental data are compared both with the CCC model calculations for ideal conditions and with the convoluted curves (Fig. 5). It can be seen that the influence of the finite system resolution is expected to be negligible, except for small scattering angles. Therefore the theories and measurements can be safely compared beyond this region. However, care should be taken when analyzing the derived quantities P^+ and $\overline{P_\ell}$ that are strongly affected by these effects at scattering angles around $0°$. These results confirm the major conclusions on the effect of finite angular resolution made by Zetner *et al.* [44].

As seen from the graphs, the agreement between the experiment and the CCC calculations is excellent at the scattering angles from 15° to 140°. The CCC calculations modified for finite angular effects accurately reproduce the behavior of the scattering parameters observed at smaller angles. Minor discrepancies between the experiment and theory in most cases are comparable to the combined value of systematic and statistical experimental uncertainties.

The distorted-wave localized exchange model calculations (DWB1LE) by Mathur [45] are shown in Fig. 5 for $L_\perp$, γ, and P^+ parameters. Clearly there are difficulties with the theory in the intermediate range of scattering angles for all parameters. The second-order distorted-wave calculations (DWB2) of Madison *et al.* [46] have not improved the situation substantially. The model describes only the general trends in the behavior of $L_\perp$ and γ. The structure predicted by this theory for $\overline{P_\ell}$ and P^+ at the intermediate angles has not been observed experimentally. These comparisons demonstrate the generally poor accuracy of both distorted-wave calculations. A small difference in the electron energy used in the calculations (20 eV) and experiments (21.8 eV) cannot explain the significant qualitative discrepancies between the distorted-wave theories and the present measurements.

It is interesting to compare the situation for two different alkali-metal atoms, sodium and lithium, reviewed by Andersen *et al.* [19]. The case of sodium is investigated very well both theoretically and experimentally. Taking the DWB2 model as an example of the most sophisticated distorted wave theory [47], we note that it provides reasonably good quantitative agreement with both the experimental results and the CCC model when applied to sodium at the range of energies about 20 eV. Even for 12 eV the DWB2 predictions are correct for the spin-averaged parameters. Nevertheless, this model fails to describe the behavior of the alignment and orientation parameters at 21.8 eV in lithium when compared to the present experimental data (Fig. 5). Despite its simpler atomic structure, lithium appears to be a more difficult target for the distorted-wave-based electron-atom scattering theories than the more complex sodium atom.

The structure that is seen in the reduced polarization parameter P^+ is very similar to that reported by Teubner and Scholten [48] in their superelastic-scattering experiment in sodium. The authors attribute the structure to a manifestation of significant exchange amplitudes in the scattering process. They also proposed a simple wave mechanical model that can be applied in the present case. In particular this model predicts that significant departure from $P^+=1$ will be most apparent near the minimum in the differential cross sections and at low energies. It also predicts that the structure will move to large scattering angles as the energy decreases. The

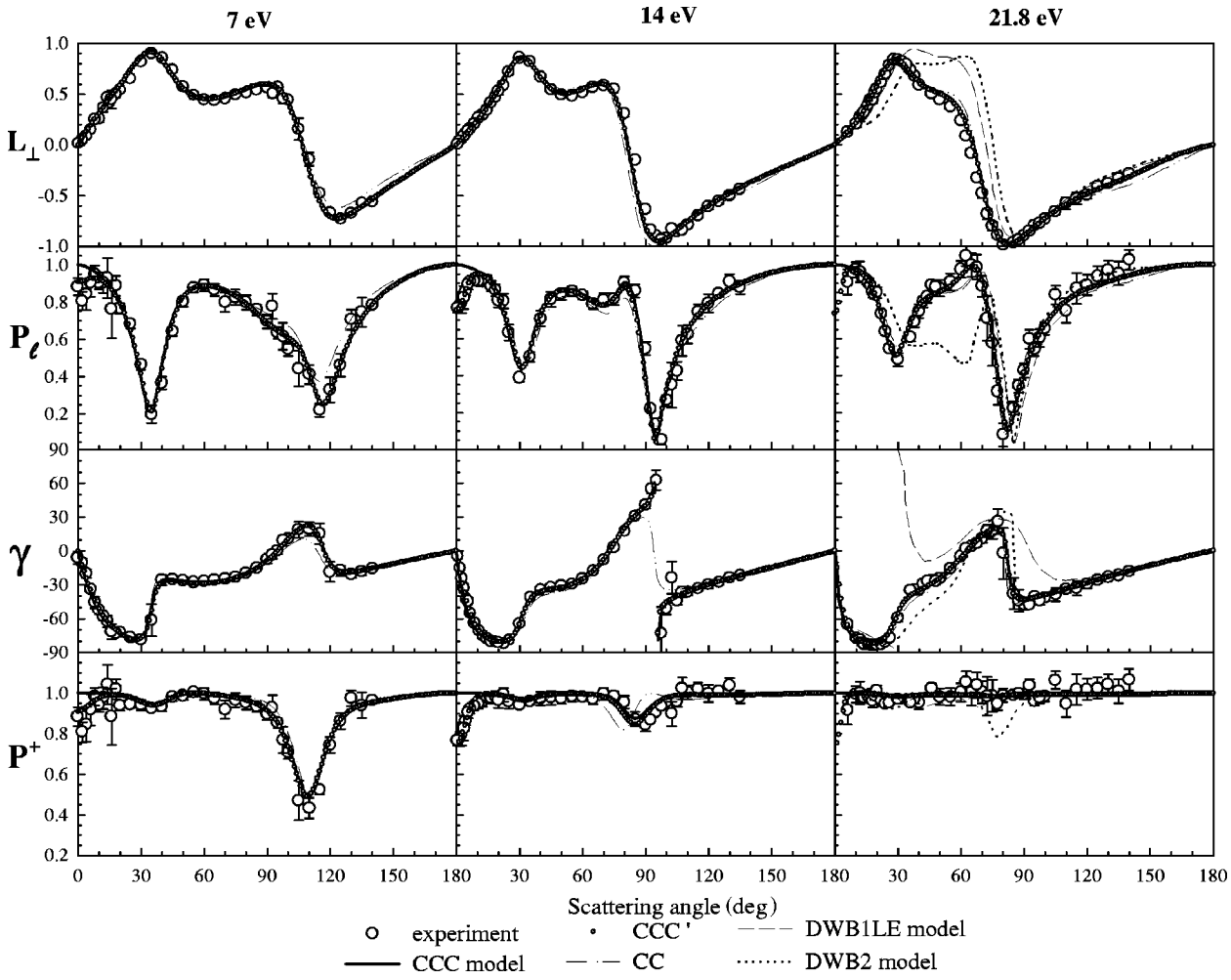

FIG. 5. Orientation parameter $L_\perp$, alignment parameters γ and $\overline{P}_\ell$, and coherence parameter P^+ measured for electron energies of 7, 14, and 21.8 eV referred to the ground state. The uncertainties represent plus and minus one standard deviation. The convergent close-coupling results denoted by CCC have been convoluted with the experimental angular resolution to obtain the curve denoted by CCC′. The DWB1LE and DWB2 data are adapted from the review by Andersen *et al.* [19] and given for an electron energy of 20 eV.

present results for P^+ demonstrate that the simple model can be used to provide a qualitative description of the scattering process in electron scattering from lithium. We note that there is excellent agreement between the measured P^+ and that predicted by the CCC. This level of agreement reflects the excellent agreement between theory and experiment that was observed for the Stokes parameters that comprise P^+.

V. CONCLUSIONS

Neither distorted-wave model accurately predicts all of the measured values of orientation and alignment parameters obtained in the present project. In contrast, the convergent close-coupling calculations are found to be in excellent quantitative agreement with the experiments over the whole range of the scattering angles.

The differential cross sections were also determined in our experiments by studying the $2P$-$2S$ superelastic-scattering process. The measured values appeared to be in better agreement with the CCC calculations than previously reported experimental results [8,9] obtained using the conventional inelastic-scattering technique.

The predictions of the CCC model for sodium have proved to be very accurate [42]. The present study has confirmed the validity of this theory for lithium, the lighter open-shell atom, for electron energies of 7, 14, and 21.8 eV. When the project began there was reason to suspect that the CCC theory may not work as well for the lithium target due to the discrepancy with some of the e-H scattering experiments. Present e-Li measurements and the recent e-H measurements [2,3] suggest that the CCC theory is equally valid for all these targets.

ACKNOWLEDGMENTS

This work was supported by the Australian Research Council. One of us (V.K.) gratefully acknowledges the support of the Overseas Postgraduate Research Scheme and Flinders University. We wish to thank Dr. P. Farrell for helpful discussions. We are also indebted to the South Australian Center for High Performance Computing and Communications.

[1] V. Karaganov, I. Bray, P. J. O. Teubner, and P. Farrell, Phys. Rev. A **54**, R9 (1996).
[2] H.-A. Yalim, D. Cvejanovic, and A. Crowe, Phys. Rev. Lett. **79**, 2951 (1997).
[3] R. W. O'Neill, P. J. M. van der Burgt, D. Dziczek, P. Bowe, S. Chwirot, and J. A. Slevin, Phys. Rev. Lett. **80**, 1630 (1998).
[4] N. Andersen, J. W. Gallagher, and I. V. Hertel, Phys. Rep. **165**, 1 (1988).
[5] I. P. Zapesochnyi, E. N. Postoi, and I. S. Aleksakhin, Zh. Éksp. Teor. Fiz. [Sov. Phys. JETP **41**, 865 (1975)].
[6] D. Leep and A. Gallagher, Phys. Rev. A **10**, 1082 (1974).
[7] B. Jaduszliwer, A. Tino, B. Bederson, and T. M. Miller, Phys. Rev. A **24**, 1249 (1981).
[8] W. Williams, S. Trajmar, and D. Bozinis, J. Phys. B **9**, 1529 (1976).
[9] L. Vušković, S. Trajmar, and D. F. Register, J. Phys. B **15**, 2517 (1982).
[10] T. Shuttleworth, D. E. Burgess, M. A. Hender, and A. C. H. Smith, J. Phys. B **12**, 3967 (1979).
[11] G. Baum, M. Moede, W. Raith, and U. Sillmen, Phys. Rev. Lett. **57**, 1855 (1986).
[12] G. Baum, L. Frost, W. Raith, and U. Sillmen, J. Phys. B **22**, 1667 (1989).
[13] I. Bray, D. V. Fursa, and I. E. McCarthy, Phys. Rev. A **47**, 1101 (1993).
[14] V. Karaganov, I. Bray, and P. J. O. Teubner, J. Phys. B **31**, L187 (1998).
[15] D. F. Register, S. Trajmar, S. W. Jensen, and R. T. Poe, Phys. Rev. Lett. **41**, 749 (1978).
[16] Y. Li and P. W. Zetner, J. Phys. B **29**, 1803 (1996).
[17] P. W. Zetner, S. Trajmar, S. Wang, I. Kanik, G. Csanak, R. E. H. Clark, J. Jr. Abdallah, and J. C. Nickel, J. Phys. B **30**, 5317 (1997).
[18] T. Y. Jiang, Z. Shi, C. H. Ying, L. Vušković, and B. Bederson, Phys. Rev. A **47**, 1101 (1993).
[19] N. Andersen, K. Bartschat, J. T. Broad, and I. V. Hertel, Phys. Rep. **279**, 251 (1997).
[20] K. J. Ross and B. Sonntag, Rev. Sci. Instrum. **66**, 4409 (1995).
[21] A. N. Nesmeyanov, *Vapour Pressure of the Chemical Elements* (Elsevier, Amsterdam, 1963).
[22] J. A. Simpson, Rev. Sci. Instrum. **32**, 1283 (1961).
[23] W. Jitschin, Appl. Phys. B: Photophys. Laser Chem. **B33**, 7 (1984).
[24] J. F. Kelly and A. Gallagher, Rev. Sci. Instrum. **58**, 563 (1987).
[25] R. E. Scholten, G. F. Shen, and P. J. O. Teubner, J. Phys. B **26**, 987 (1993).
[26] P. M. Farrell, W. R. MacGillivray, and M. C. Standage, Phys. Rev. A **44**, 1828 (1991).
[27] N. Andersen and I. V. Hertel, Comments At. Mol. Phys. **19**, 1 (1986).
[28] X.-K. Meng, W. R. MacGillivray, and M. C. Standage, Phys. Rev. A **45**, 1767 (1992).
[29] P. J. O. Teubner, V. Karaganov, M. R. Law, and P. M. Farrell, Can. J. Phys. **74**, 984 (1996).
[30] P. M. Farrell (private communication).
[31] H. W. Hermann and I. V. Hertel, Comments At. Mol. Phys. **12**, 127 (1982).
[32] J. Mitroy, I. E. McCarthy, and A. T. Stelbovics, J. Phys. B **20**, 4827 (1987).
[33] K. E. Martus, K. Becker, and D. H. Madison, Phys. Rev. A **38**, 4876 (1988).
[34] P. W. Zetner, S. Trajmar, and G. Csanak, Phys. Rev. A **41**, 5980 (1990).
[35] K. Becker, A. Crowe, and J. W. McConkey, J. Phys. B **25**, 3885 (1992).
[36] R. T. Sang, P. M. Farrell, D. H. Madison, W. R. MacGillivray, and M. C. Standage, J. Phys. B **27**, 1187 (1994).
[37] R. T. Sang, Ph.D. thesis, Griffith University, Brisbane, 1995 (unpublished).
[38] S. J. Buckman, P. Hammond, G. C. King, and F. H. Read, J. Phys. B **16**, 4219 (1983).
[39] K. Kadota, D. Dijkkamp, R. L. vander Woude, A. de Boer, Pan Guang Yan, and F. J. de Heer, J. Phys. B **15**, 3275 (1982).
[40] R. E. Scholten, V. Karaganov, P. M. Farrell, and P. J. O. Teubner, Phys. Rev. A (to be published).
[41] M. Born and E. Wolf, *Principles of Optics* (Pergamon, London, 1970).
[42] I. Bray, Phys. Rev. A **49**, 1066 (1994).
[43] D. Leep and A. Gallagher, Phys. Rev. A **10**, 1082 (1974).
[44] P. W. Zetner, Y. Li, and S. Trajmar, J. Phys. B **25**, 3187 (1992).
[45] K. C. Mathur, Phys. Rev. A **39**, 903 (1989).
[46] D. H. Madison, R. P. McEachran, and M. Lehmann, J. Phys. B **27**, 1807 (1994).
[47] D. H. Madison, K. Bartschat, and R. P. McEachran, J. Phys. B **25**, 5199 (1992).
[48] P. J. O. Teubner nd R. E. Scholten, J. Phys. B **25**, L301 (1992).